Journal of Materials Chemistry

Cite this: J. Mater. Chem., 2011, 21, 13490

www.rsc.org/materials

PAPER

Chitosan/NiO nanocomposites: a potential new dielectric material†

Aarti Sripathi Bhatt,[a] Denthaje Krishna Bhat,*[a] Mysore Sridhar Santosh[a] and Cheuk-wai Tai[b]

Received 7th May 2011, Accepted 6th July 2011
DOI: 10.1039/c1jm12011e

The study of electrochemical behavior of organic–inorganic nanocomposite materials remains a major challenge for application in energy storage devices. Here, new composite materials of chitosan and NiO nanoparticles have been fabricated. The NiO nanoparticles are well characterized by infrared spectroscopy, X-ray diffraction and transmission electron microscopy. The electrical properties of the films are studied by impedance spectroscopy at different temperatures; and thereby permittivity, electric modulus and conductivity data are obtained. By studying the variations in permittivity and electric modulus spectra with respect to applied frequency signal and temperature, the ionic conductivity of the material is investigated. The Correlated Barrier Hopping model is employed to understand the conduction mechanism. An admirable conductivity of 1.4×10^{-2} S cm^{-1} is obtained for a nanocomposite with 4 wt% NiO content. The activation energies of the composite films decrease with increase in NiO content, from 16.5 to 4.8 kJ mol^{-1}.

1. Introduction

The use of inorganic "nano-fillers" into the polymer matrix can lead to novel high performance composite materials. Popular applications of polymer–inorganic nanocomposites include mechanical, biomedicinal, optical, catalysis, magnetic, thermal, electrical and electrochemical applications. Electronic technologies that allow for a reduction in size, weight and cost while improving the functionality and performance are highly desired for commercial purposes. Metal filled polymer composites have the potential to address the needs of emerging dielectric technologies. In an applied field, dipoles formed in each of the metal particles result in polarization that simulates a true dielectric. For high frequency applications, engineering small particles with high electron mobilities is essential since only these properties will enable the rapid field response necessary for high dielectric constant and low loss. These nanocomposite dielectrics have the competence to have high dielectric constants at high frequencies and to enable the low temperature processing associated with polymers. This combination of properties is not found in other capacitor materials.

Though the choice of polymer matrix is manifold, we preferred chitosan for our present work, mainly because of its easy availability, low cost, environment friendly nature and superior mechanical properties. For the same reasons, chitosan is being widely used by the research community in the recent times.[1–4] Frequently employed inorganic nano-fillers for electrical and electrochemical applications include metal oxides like ZnO, SiO, TiO_2[5] and recently carbon-based materials like carbon nanotubes (CNT) and graphites[6] are also being employed. However, there are only a handful of papers wherein the dielectric properties of NiO have been exploited in the form of nano-fillers. In its bulk form, NiO has a cubic (NaCl type) structure with a lattice parameter of 0.4177 nm and is classified as Mott–Hubbard insulator with very low conductivity of the order of 10^{-11} ohm^{-1} m^{-1} at room temperature.[7,8] However, the conductivity drastically increases when the size is reduced to nanoscale,[9] wherein the electrical conduction is mainly due to hopping of holes associated with Ni^{2+} vacancies. Adding these fillers into nonconductive polymers can make the polymer electrically conductive while still retaining their polymeric characteristics. For example, Yuan *et al.* have reported an increase in conductivity when NiO nanoparticles were supported on mesocarbon microbeads (MCMBs). They further showed that these NiO/MCMB composites have excellent supercapacitive behaviours.[10] The dielectric behavior of Li and Ti co-doped NiO/PVDF composites was studied by Dang and Nan.[11] Furthermore, it is possible to understand the mechanism of conduction by studying the variations in dielectric properties and electric modulus. Presently, there is a lack of literature citing the electrochemical behavior of such nanocomposites.

Keeping in view the above, we intend to coalesce the benefits of NiO nanoparticles into chitosan polymer matrix. In precise, the present study includes two main aspects: (1) to prepare and characterize chitosan/NiO nanocomposite polymer films. NiO nanoparticles were synthesized by hydrothermal route and the nanocomposite films were prepared by solution casting. (2) To

[a]*Department of Chemistry, National Institute of Technology Karnataka, Surathkal, Srinivasnagar, 575025, India. E-mail: denthajekb@gmail.com*
[b]*Division of Inorganic and Structural Chemistry, Department of Materials and Environmental Chemistry, Arrhenius Laboratory, Stockholm University, S-10691 Stockholm, Sweden*
† Electronic supplementary information (ESI) available. See DOI: 10.1039/c1jm12011e

study the influence of NiO nano-fillers on the electrochemical behavior of the polymer matrix.

2. Experimental

The chemicals nickel acetate tetrahydrate (Sigma-Aldrich) and urea (Merck) used in the preparation of nickel oxide nanoparticles were of analytical grade and were used without any further purification. Polyethylene glycol (PEG) of molecular weight 10 000 and medium molecular weight chitosan were provided by Sigma-Aldrich and were used as received. Distilled water was used throughout the study.

2.1. Synthesis of NiO nanocomposites

The synthesis of NiO nanoparticles involved the preparation of precursor using hydrothermal method. 1 g of nickel acetate and 1 g of urea were dissolved in 10 ml distilled water. To this 4 g PEG was added and the solution was stirred with a magnetic stirrer at room temperature for one hour to obtain a homogeneous solution. Thereafter the mixture was transferred to a Teflon lined autoclave and heated at 453 K for 3 h. The light green coloured precipitate was centrifuged several times by giving alternate wash with water and alcohol and then dried at 333 K for 6 h. The obtained precursor was then calcined at 673 K for 3 h to yield the dark green coloured NiO nanoparticles.

2.2. Preparation of chitosan/NiO nanocomposites

First, chitosan solution in 2% acetic acid solution (2% m/v) was prepared. For this, 500 mg of chitosan was dissolved in 25 ml of the solvent and the solution was sonicated for about 6 h. After the complete dissolution of chitosan, NiO nanoparticles were then added to it and the solution was again subjected to sonication. On complete dispersion of NiO nanoparticles, the solution was solution cast on glass Petri dishes and dried at 333 K for 24 h. The films formed were further soaked in distilled water for 24 h to remove residual solvent. For simplicity, the nanocomposite films were labeled as CNH0, CNH1, CNH2 and CNH3 for 0 wt%, 2 wt%, 4 wt% and 6 wt% respectively. Addition of NiO higher than 6 wt% leads to a heterogeneous solution.

2.3. Characterisation

FTIR (THERMO) spectrophotometer has been used to determine the formation of the nanoparticles from the precursor. The X-ray powder diffraction analysis was conducted on a JEOL X-ray Diffractometer at a scanning rate of 2° per minute with 2θ ranging from 20 to 80°, using Cu K_α radiation ($\lambda = 1.5406$ Å). Electrochemical impedance measurements were carried out using an electrochemical work station, AUTOLAB 30. The films were placed in between two stainless electrodes. The whole set up was held tightly with a plastic clamp. 1 M KOH solution was used as electrolyte. Experiments were carried out at room temperature and at higher temperatures (313–343 K). An oil bath was used to maintain the required constant temperature. The measurements were carried out using a small amplitude AC signal of 10 mV over a frequency range of 100 kHz to 0.01 Hz. Minimum three trials were taken for each reading.

3. Results and discussions

3.1. XRD analysis

From the fundamental FTIR spectroscopy studies, the presence of metal–oxygen bonds in the final sample after calcination was established (see Fig. S1, ESI†, for details and related discussion). The XRD pattern of the calcined sample matched well with the JCPDS file no 47-1049 corresponding to cubic NiO (Fig. 1). Moreover, the broad base of each of these peaks suggests the nanosize of the particles. Using the Debye–Scherrer equation, the estimated average particle size was found to be 10 nm. Fig. 1 also shows the XRD patterns of nanocomposite films. The presence of (200) (marked by an asterisk) diffraction peak in each of the films confirms the successful incorporation of the nanoparticles.

3.2. TEM measurements

Fig. 2a shows the TEM image of NiO nanoparticles. The image shows aggregation due to sintering, which is a common phenomenon when amorphous nanoparticles are calcined. From different TEM micrographs, the average diameter of NiO nanoparticles, D_{TEM}, was found to be 9 nm over 200 particles (Fig. 2b). This is in good agreement with the result obtained in the XRD measurement. The selected area diffraction pattern (SAED) (Fig. 2c) reveals that the sample is polycrystalline with ring patterns which can be indexed to NiO cubic structure. The d space values measured from SAED patterns are listed in Table 1. The d values of the bulk NiO are also given for comparison. It is clear that the values of the synthesized nanoparticles match very well with the standard references. A small deviation seen in the lattice parameters is usually observed in nanomaterials. No other ring pattern corresponding to any kind of impurities is observed. This confirms that the crystal structure is pure NiO with cubic structure and $Fm2m$ space group. From the assigned d values the lattice parameter, a, was estimated to be 0.4169 nm, which is close to that of bulk NiO (0.4195 nm). A small deviation in the value of lattice parameter from the bulk is usually common in nanomaterials.

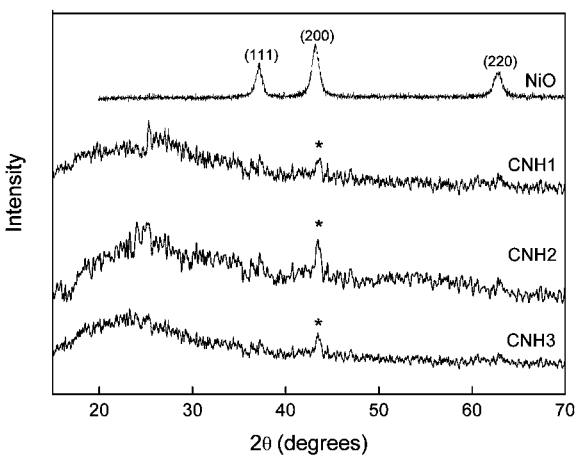

Fig. 1 XRD patterns of NiO nanoparticles and chitosan/NiO films.

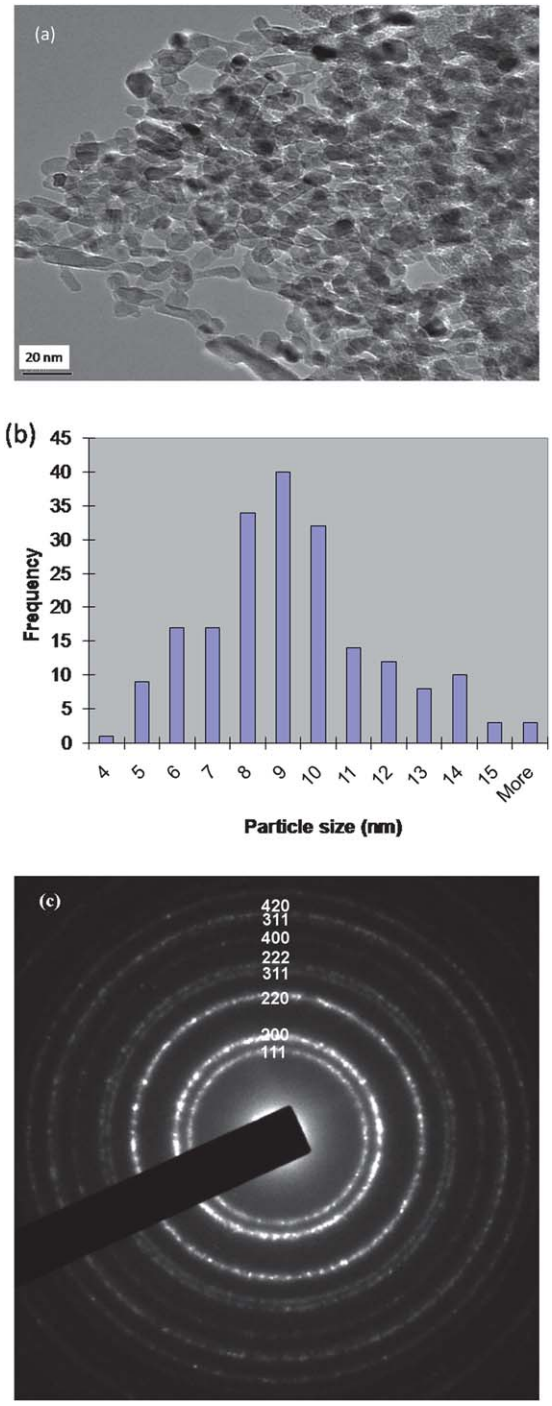

Fig. 2 (a) TEM image, (b) size distribution histogram and (c) SAED pattern of NiO nanoparticles.

3.3. Magnetic measurements

Bulk NiO is known to be antiferromagnetic (AFM) below Neel temperature, T_N = 523 K. Different kinds of magnetic phase mainly depend on sign and relative strength of the nearest neighbor and the next nearest neighbor exchange interactions.[12] Magnetic characterization of the samples was performed by magnetic hysteresis measurements at room temperature. The magnetization (M) as a function of applied magnetic field (H) for NiO nanoparticles is shown in Fig. 3a. The shape of the magnetic curve is similar to those reported by Ghosh *et al.*[13] and the room temperature magnetization observed was 0.22 emu g^{-1}. The existence of hysteresis loop (a low coercive force and remanent magnetization) at room temperature indicates the existence of a weak ferromagnetic phase. The Ni^{2+} vacancies may be the reason for hysteresis. The AFM structure of NiO consists of two spin sublattices. Each sublattice exhibits ferromagnetic order along the (111) direction. The moments of

Table 1 Comparison of d space values (Å) for NiO

		Bulk NiO	
(h k l)	This study	Ref. 1[a]	Ref. 2[b]
(1 1 1)	2.40	2.40	2.41
(2 0 0)	2.08	2.08	2.09
(2 2 0)	1.47	1.47	1.48
(3 1 1)	1.26	1.26	1.26
(2 2 2)	1.20	1.20	1.21
(4 0 0)	1.04	1.04	—
(3 3 1)	9.58	9.60	—
(4 2 0)	9.31	9.30	—

[a] ICSD 00-001-1239. [b] ICSD 01-073-1523.

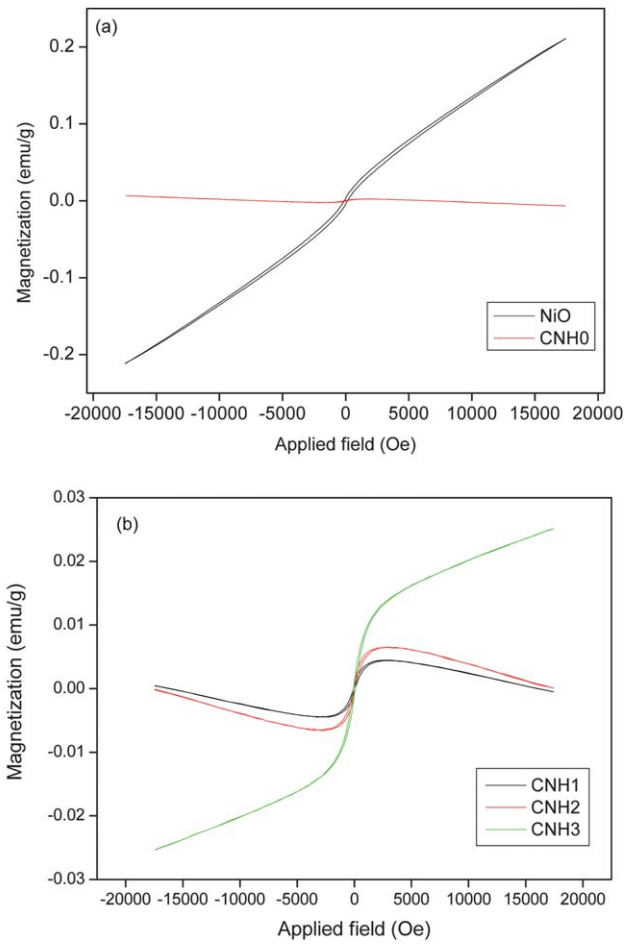

Fig. 3 Room temperature magnetization curves for (a) NiO nanoparticles and blank chitosan film and (b) chitosan/NiO nanocomposite films.

adjacent sublattices are aligned in the opposite direction to generate an AFM structure. With the reduction in the size of NiO particles to nanoscale, the density of Ni vacancies in NiO lattice increases; thereby partially destroying the AFM spin order and favouring a ferromagnetic spin order. Also due to the larger surface area of the nanoparticles, a certain amount of uncompensated spins may remain on the surface giving rise to hysteresis.[14]

The magnetic properties of chitosan/NiO composite samples were also studied. Fig. 3b shows the room temperature magnetization curves for the composite films. The saturation magnetization of the composite films depends on the amount of magnetic phase added to it. With the increase in the content of nanoparticles, the saturation magnetization also increased. A blank chitosan film exhibited a diamagnetic behavior with a room temperature magnetization of 0.002 emu g^{-1} (Fig. 3a). Subtracting the diamagnetic contribution from the composite films, the magnetization for CNH1, CNH2 and CNH3 corresponds to 0.0026 emu g^{-1}, 0.0043 emu g^{-1} and 0.024 emu g^{-1} respectively. The saturation magnetization for CNH1 and CNH2 films is consistent with the amount of NiO added, thereby suggesting a homogeneous distribution of NiO nanoparticles. However in the case of CNH3, the magnetization value is higher than expected. Smaller size of the particles may allow a much more homogeneous distribution, but a higher content may induce aggregation due to high specific surface area of nanoparticles, thus lowering the homogeneity of particle distribution. As mentioned earlier in Section 2.2, addition of NiO content more than 6 wt% failed to yield a good homogeneous composite film. Thus, we can say that at lower content of NiO, the dispersion of nanoparticles is uniform. However, aggregation initiates on addition of 6 wt% NiO and more. Since the synthesized NiO nanoparticles are less than 10 nm, the aggregation at higher content of nanoparticles is not surprising. Xu and others have also observed a similar trend and have attributed this to the increasing tendency of the nanoparticles to aggregate on increasing their content.[15] Compared to the nanoparticles, the magnetization value of the composites is little; nevertheless it is not negligible.

3.4. Electrochemical studies

Electrochemical impedance spectroscopy is of considerable importance for deducting material properties like conductivity, dielectric properties and electric modulus. In the present study, the real (Z') and imaginary (Z'') part of complex impedance (Z^*) were used for the evaluation of real (ε'/M') and imaginary (ε''/M'') parts of complex dielectric (ε^*) and complex electric modulus (M^*) using eqn (1)–(5).

$$Z^* = Z' + jZ'' \quad (1)$$

$$\varepsilon' = \frac{Z''}{\omega C_0\left(Z'^2 + Z''^2\right)} \quad (2)$$

$$\varepsilon'' = \frac{Z'}{\omega C_0\left(Z'^2 + Z''^2\right)} \quad (3)$$

$$M' = \frac{\varepsilon'}{\left(\varepsilon'^2 + \varepsilon''^2\right)} \quad (4)$$

$$M'' = \frac{\varepsilon''}{\left(\varepsilon'^2 + \varepsilon''^2\right)} \quad (5)$$

Here $C_0 = \varepsilon_0 A/t$ and ε_0 is the permittivity of free space, A is the electrolyte–electrode contact area and t is the thickness of the sample and $\omega = 2\pi f$, f being the frequency in Hz.

An equivalent circuit of 3 elements (see Fig. S2, ESI†) was used to simulate the measured impedance data. It consists of two constant phase elements (CPEs) Q in parallel with each other and a resistor R in series with one of the CPEs. Fig. 4 shows the complex impedance plots of pure chitosan and chitosan/NiO composite films at different temperatures. The calculated charge transfer resistance (R_{ct}) values of the films at various temperatures are given in Table 2. It is interesting to note that the bulk resistance of pure chitosan is higher than that of composite films. Among the composite films, the resistance decreases with increase in the amount of nanoparticles. Also, it can be noticed that the resistance decreases with rise in temperature from 303 K to 343 K. All this collectively shows the dominance of NiO nanoparticles in the electrolyte film.

3.4.1. Dielectric studies. The real and imaginary parts of the dielectric constant were deduced using eqn (2) and (3). The variations of ε' and ε'' with frequency at different temperatures for PC and CNH1 are shown in Fig. 5 and 6, respectively. From the figures it is seen that the dielectric constant decreases with increasing frequency. A similar trend is observed for the other two nanocomposite films. Generally, the dielectric behavior in nanostructured materials is due to different types of polarizations present in the material.[16] The interfaces of nanostructured materials possess large number of defects which can cause a change of positive or negative space charge distribution. In the presence of an electric field, these space charges move and get trapped giving rise to dipole moments. This is called space charge polarization. As the temperature increases, more and more dipoles will be oriented, resulting in an increase in the value of the dipole moment.[17] And so the dielectric constant increases with increase in temperature for fixed frequencies. A similar observation can be derived for the imaginary value of permittivity (Fig. 6). ε'' is the measure of energy spent during polarization.[18] More about the significance of ε'' will be discussed in the following section.

3.4.2. Electric modulus. The electric modulus spectra provide an opportunity to investigate conductivity and its associated relaxation in ionic conductors and polymers.[19] Basically, electric modulus is reciprocal of permittivity $M^* = 1/\varepsilon^*$. Physically, the electric modulus corresponds to the relaxation of the electric field in the material when the electric displacement remains constant. It was originally introduced by Macedo *et al.*[20] to study space charge relaxation phenomena. But in the recent years, its usage has been extended to analyse ionic conductivities.[21] A combined study of complex modulus and permittivity is beneficial to interpret the conduction

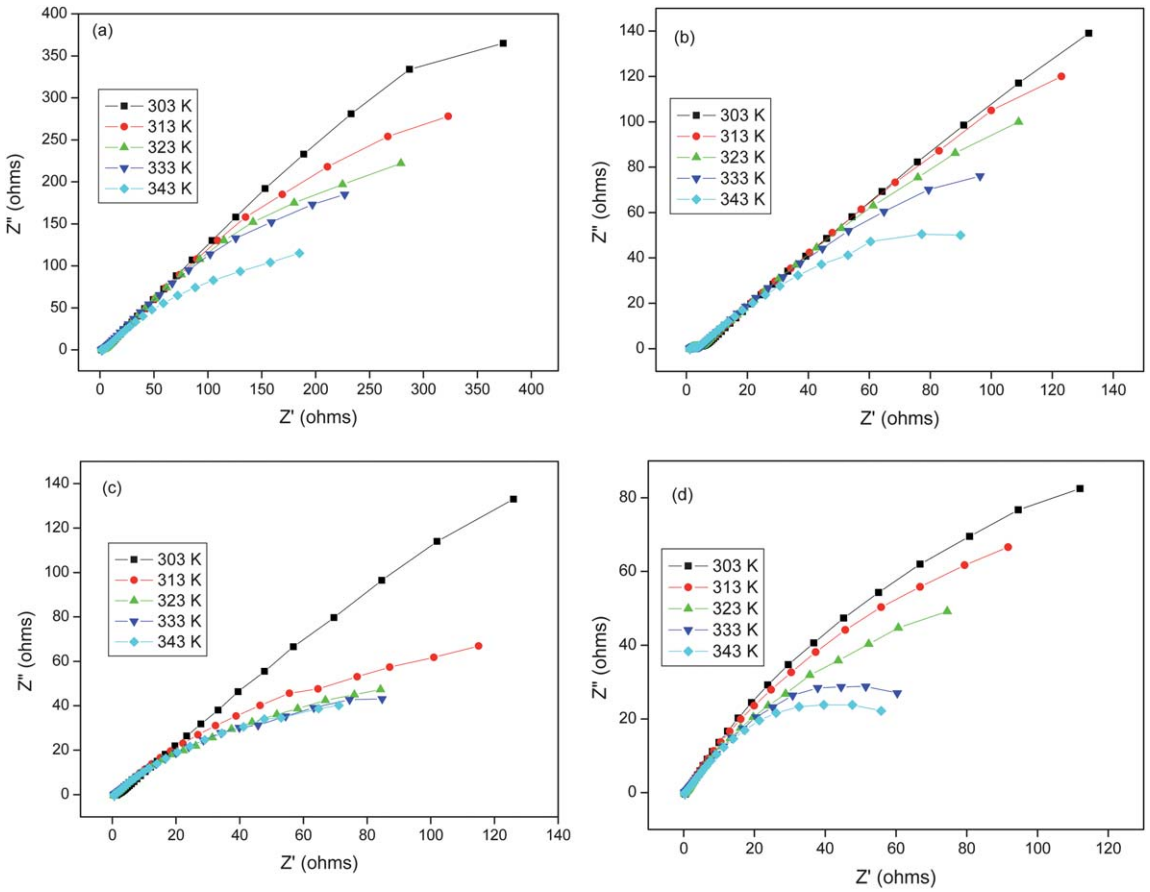

Fig. 4 Nyquist plots for (a) PC, (b) CNH1, (c) CNH2 and (d) CNH3 at different temperatures.

phenomena. Generally for a pure conduction process, a relaxation peak would be observed in the frequency spectra of the imaginary component M^* and no peak would take place in the corresponding plot of ε^*. However, for a dielectric relaxation process, a relaxation peak appears both in M^* and ε^* representations. Comparisons of ε^* and M^* representations have been used to distinguish localized dielectric relaxation processes from long range conductivity.[22,23]

Fig. 7 shows the frequency dependence of M'' spectra for different nickel oxide concentrations at 303 K. A broad relaxation peak is observed for the sample CNH1. However, no such prominent peak is observed for the other two composite films. The disappearance of peaks for films with higher metal oxide concentration may be due to the large amount of free charge carrier concentration and their motions within the material. The peak represents the conductivity relaxation peak for the distribution of relaxation times of the free charges and the broad nature of the peak suggests a non-Debye type of relaxation in the material.[24]

Fig. 8 shows the frequency dependence of the real and imaginary parts of the electric modulus at higher temperatures for the sample CNH1. From Fig. 8a, it is obvious that at lower frequencies M' values are very small indicating the removal of electrode polarization.[25,26] The increase of M' with increasing frequency and reaching a maximum value M_∞ at high frequency may be due to the distribution of relaxation processes over a range of frequencies.[27] The absence of any relaxation peak in M' is because M' in complex electric modulus (M^*) is equivalent to ε' in complex permittivity (ε^*). In other words, M' represents the ability of the material to store energy. The reduction in the values of M' with increasing temperatures results from the increase in the mobility of the polymer segment and charge

Table 2 R_{ct} values (in ohms) for pure and composite films at different temperatures

Temp./K	PC	CNH1	CNH2	CNH3
303	1.0304×10^4	2.6334×10^3	1.5543×10^3	3.4226×10^2
313	1.3382×10^3	1.3068×10^3	2.5352×10^2	2.7601×10^2
323	8.4561×10^2	7.3131×10^2	2.1250×10^2	1.9574×10^2
333	7.6781×10^2	4.2253×10^2	1.9144×10^2	9.8332×10^1
343	5.7607×10^2	2.0637×10^2	1.7556×10^2	8.0356×10^1

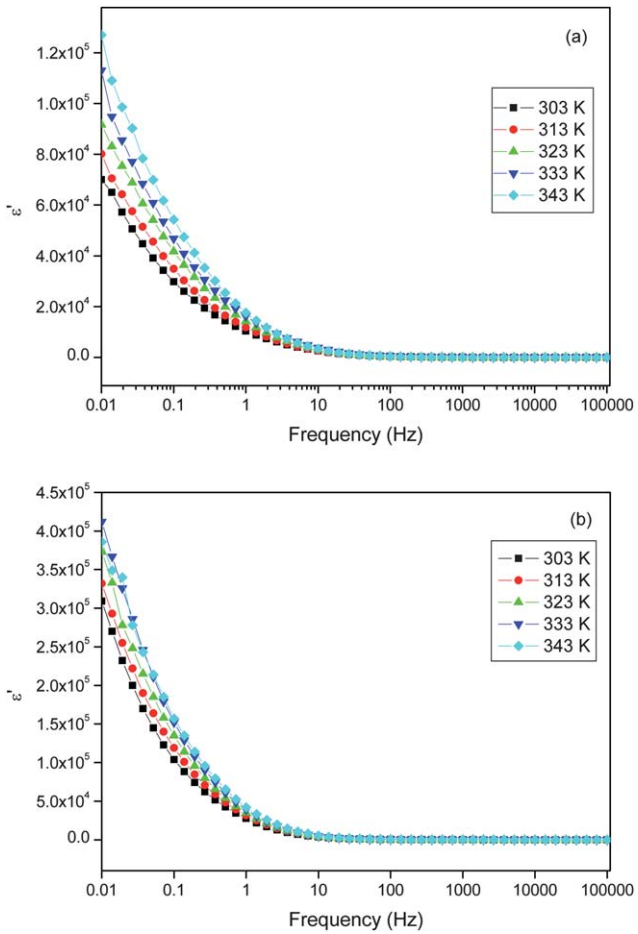

Fig. 5 Frequency variation of ε' for (a) PC and (b) CNH1 films at different temperatures.

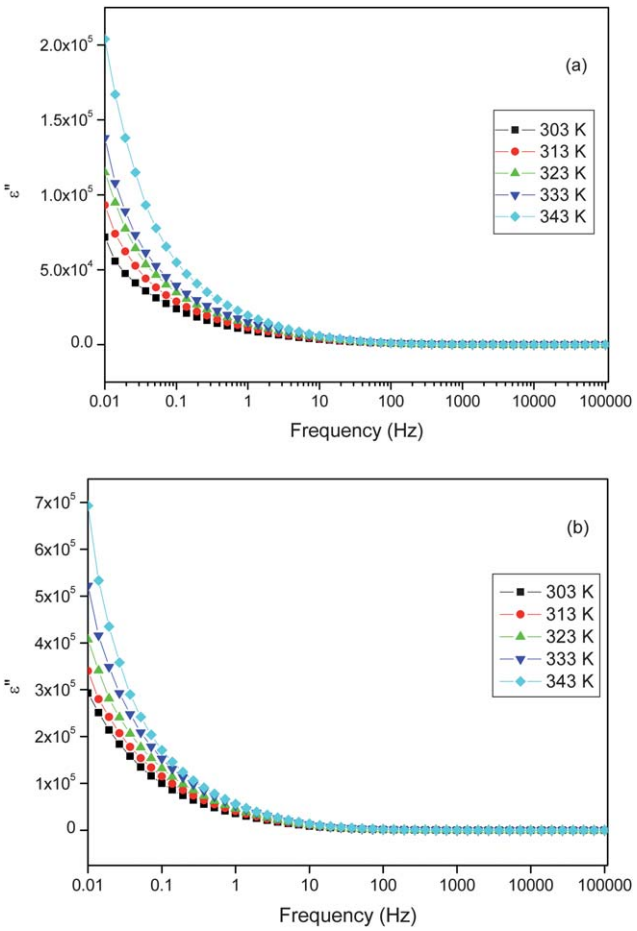

Fig. 6 Frequency variation of ε'' for (a) PC and (b) CNH1 films at different temperatures.

carriers with the temperature.[28] It is well known that the orientation of the charge carriers and molecular dipoles becomes easier at higher temperatures.

Fig. 8b shows the variation in the imaginary part of the complex modulus with frequency at higher temperatures. At lower frequencies M'' exhibits low values, which might be due to the large value of capacitance associated with the electrode polarization effect[29] as a result of accumulation of a large amount of charge carriers at the electrode/solid polymer electrolyte interface. At the higher frequencies, no well defined peaks are observed. Nevertheless, there does appear the formation of loss peaks. The partial appearance of loss peaks is due to experimental frequency limitations. The broad nature of the peaks predicts a non-Debye behavior. The absence of any relaxation peak in the corresponding plot of ε^* ascertains a conduction process for the chitosan/NiO system.

3.4.3. Conductivity. The bulk ionic conductivities of the nanocomposite films were determined from the complex impedance spectra using the equation, $\sigma = \frac{L}{RA}$ where L, A and R are the thickness, area and bulk resistance of the composite films respectively. The bulk resistance was calculated from the high frequency intercept on the real impedance axis of the Nyquist plot.[30] The temperature dependence of conductivity for the pure film and composite films is shown in Fig. 9. The conductivity increases with increasing temperature for all the composite films. This trend may be related to the increase in the drift mobility of thermally activated charge carriers (electron and hole).

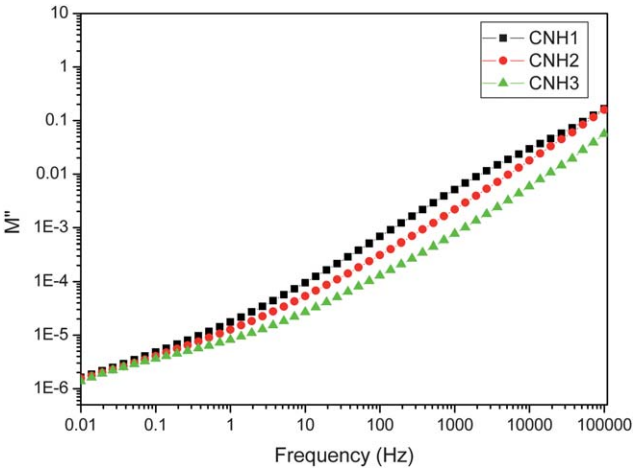

Fig. 7 Frequency variation of M'' for nanocomposite films.

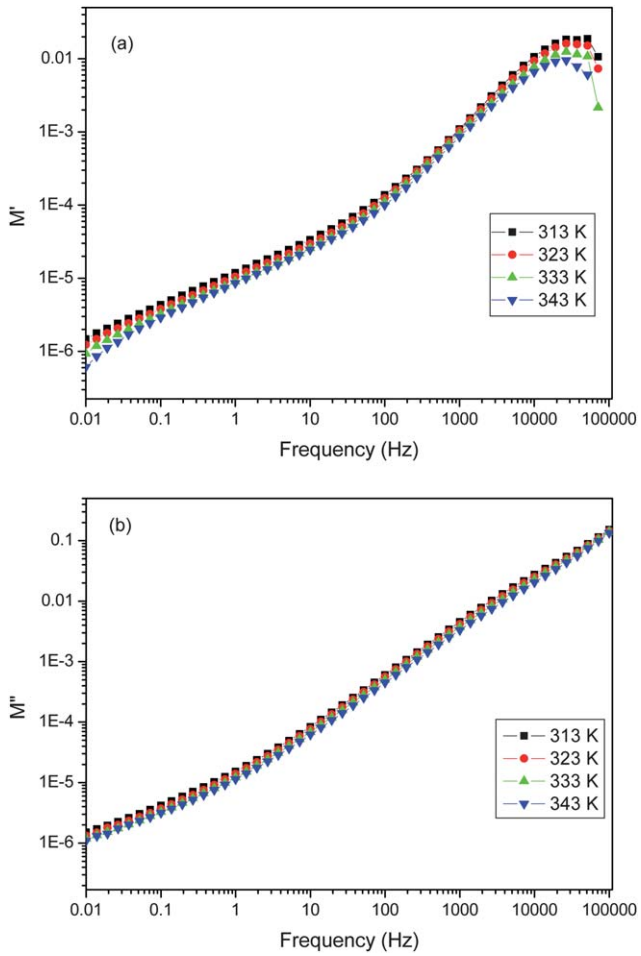

Fig. 8 Frequency variation of (a) M' and (b) M'' for CNH1 at different temperatures.

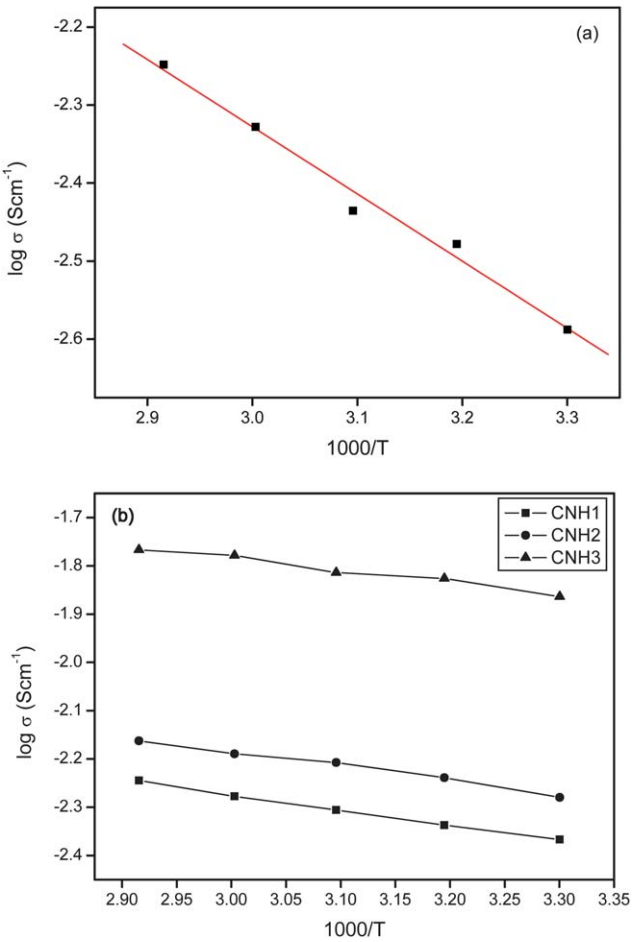

Fig. 9 Arrhenius plots for conductivity σ of (a) chitosan film and (b) composite films.

Electrical conduction is a thermally activated process and follows the Arrhenius law

$$\sigma = \sigma_0 \exp[-E_a/kT] \quad (6)$$

where σ is the conductivity at a particular temperature, σ_0 is the pre-exponential factor, k is the Boltzmann's constant and T is the absolute temperature. The activation energy can be calculated from the slope of the straight line obtained from log σ *versus* $1000/T$ and the corresponding values are listed in Table 3. The regression value R^2 lies in the range 0.97–0.99, thereby confirming that all the plotted points lie in more or less a straight line. Also, the conductivity plot does not show any abrupt jump indicating that the chitosan based nanocomposite does not exhibit any phase transition in this temperature range. The conductivity and activation energy values are plotted as a function of filler content in Fig. 10.

Activation energy is the initial energy that the electric charges need to move inside the material. It increases with temperature in insulators and semiconductors and decreases in metals. Here, E_a decreases with increase in NiO content. The decrease in E_a implies a comparatively lesser energy is required to move the charges inside the solid polymer electrolyte system. Thus it is obvious that the presence of NiO nanoparticles decreases the activation energy thereby increasing the conductivity of the polymer nanocomposites. Undoubtedly the enhancement in conductivity of nanocomposite materials is due to the presence of nanoparticles.

The conduction in chitosan/NiO can be mainly attributed to the hopping of holes associated with Ni^{2+} vacancies. However the contribution of these hopping charge carriers to polarization is not fully understood.[31] The mechanism of conductivity can be understood by studying the Correlated Barrier Hopping (CBH) model. Previously too this model has been successfully employed for interpreting the electrical conductivity data of several semiconductors.[8,32] Since in the present case NiO contributes to the conductivity to a larger extent, we propose to extend the model for the chitosan/NiO composite as a whole. In NiO, large

Table 3 Room temperature conductivity values and activation energies for the polymer films

Sample	R^2	E_a/kJ mol^{-1}	σ/S cm^{-1}
CNH0	0.987	16.49	1.30×10^{-3}
CNH1	0.998	6.04	4.30×10^{-3}
CNH2	0.988	5.66	5.25×10^{-3}
CNH3	0.974	4.82	1.37×10^{-2}

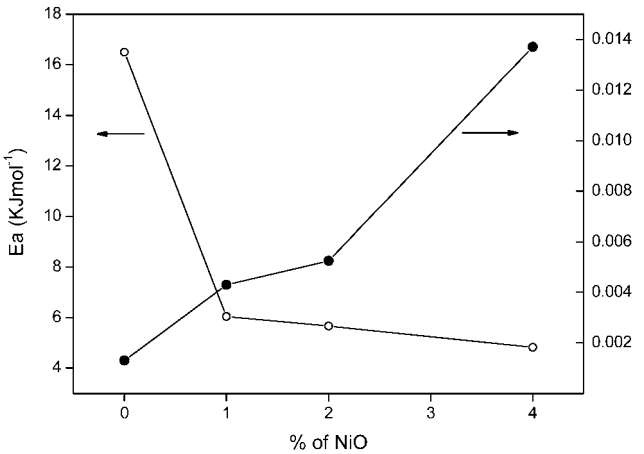

Fig. 10 Variation of activation energy E_a and room temperature conductivity σ_{RT} as a function of NiO.

conductivity is based on the presence of large number of Ni^{2+} vacancies.[7,8,32,33] The presence of a Ni^{2+} vacancy in the lattice causes the transformation of two adjacent Ni^{2+} ions into Ni^{3+} ions, in order to achieve charge neutrality. This transformation induces local lattice distortion. According to the CBH model, conduction occurs *via* a hopping process wherein two electrons simultaneously hop over the potential barrier between two charged defect sites. Two types of charge carrier movements are feasible in NiO:[32,34] (i) inter-well hopping involving the hopping of a hole from Ni^{3+} ion located in one defect potential well to a Ni^{2+} ion in an adjacent defect potential well. (ii) Intra-well hopping involving the hopping of holes between ions within one defect potential well. In the presence of an ac signal, both the mentioned charge transfer mechanisms do have a finite probability of occurrence, their relative probabilities mainly dependent on the applied frequency and the concentration of the potential wells associated with Ni^{2+} vacancies. At lower frequencies, the probability of inter-well hopping predominates over that of intra-well hopping. However, as the frequency of the applied signal is increased, the probability of occurrence of the inter-well charge transfer decreases and intra-well hopping totally takes over the conduction mechanism.[32,34] The increase in conductivity with increase in NiO content may be attributed to the higher density of Ni^{2+} vacancies and higher percolation of the potential wells associated with these Ni^{2+} vacancies.[32,34]

4. Conclusion

A completely new nanocomposite of chitosan/NiO was fabricated. Electrochemical impedance spectroscopy was carried out and thereby, the dielectric behavior of the nanocomposite films was analysed. A high permittivity was observed for the samples which decreased at higher frequencies. This is mainly due to polarization arising from the charge transfer process. A comparative study of the imaginary part of permittivity and electric modulus showed that the charge transfer is mainly by a pure conduction process. The Correlated Barrier Hopping (CBH) model could be suitably applied to the nanocomposite films. The combined mechanism of intra-well hopping and inter-well hopping satisfactorily accounts for the conductivity in the present chitosan/NiO nanocomposite materials. A maximum conductivity of 1.37×10^{-2} S cm^{-1} with corresponding activation energy of 4.82 kJ mol^{-1} was achieved for films with 6 wt% NiO content. Good dielectric behavior along with cost effectiveness and easy processibility makes these nanocomposite materials easy to be adapted in the dielectric industry.

Acknowledgements

Financial assistance in the form of an R&D project grant from DST, Govt. of India is gratefully acknowledged. A.S.B. is thankful to NITK Surathkal for the award of a research Fellowship.

References

1 M. Z. A. Yahya and A. K. Arof, *Eur. Polym. J.*, 2002, **38**, 1191–1197.
2 N. C. Mat and A. Liong, *Eng. Lett.*, 2009, **17**, 14–17.
3 S. Li, M. M. Lin, M. S. Toprak, D. K. Kim and M. Muhammed, *Nano Rev.*, 2010, **1**, 5214.
4 X. Liu, Q. Hu, Z. Fang, X. Zhang and B. Zhang, *Langmuir*, 2009, **25**, 3–8.
5 S. Ahmad, S. A. Agnihotry and S. Ahmad, *J. Appl. Polym. Sci.*, 2008, **107**, 3042–3048.
6 D. Eder, *Chem. Rev.*, 2010, **110**, 1348–1385.
7 F. G. Morin, *Phys. Rev.*, 1954, **93**, 1199–1204.
8 P. Lukenheimer, A. Loidl, C. R. Otterman and K. Bange, *Phys. Rev. B: Condens. Matter Mater. Phys.*, 1991, **44**, 5927–5930.
9 V. Biju and M. A. Khadar, *Mater. Res. Bull.*, 2001, **36**, 21–33.
10 C. Yuan, B. Gao, L. Su and X. Zhang, *Solid State Ionics*, 2008, **178**, 1859–1866.
11 Z. M. Dang and C. W. Nan, *Ceram. Int.*, 2005, **31**, 349–351.
12 M. S. Seehra and T. M. Geibultowicz, *Phys. Rev. B: Condens. Matter Mater. Phys.*, 1988, **38**, 11898–11900.
13 M. Ghosh, K. Biswas, A. Sunderasan and C. N. R. Rao, *J. Mater. Chem.*, 2006, **16**, 106–111.
14 E. L. Salabas, A. Rumplecker, F. Kleitz, F. Radu and F. Schuth, *Nano Lett.*, 2006, **6**, 2977–2981.
15 C. Xu, C. Ouyang, R. Jia, Y. Lo and X. Wang, *J. Appl. Polym. Sci.*, 2009, **111**, 1763–1768.
16 M. Chi-Mel, Z. Lide and W. Guozhong, *Nanostruct. Mater.*, 1995, **6**, 823–826.
17 T. Kar, R. N. Choudhary, S. Sharma and K. S. Singh, *Indian J. Phys., A*, 1999, **73**, 453.
18 V. V. Daniel, *Dielectric Relaxation*, Academic Press, London, 1967.
19 M. D. Migahed, M. Ishra, T. Fahmy and A. Barakat, *J. Phys. Chem. Solids*, 2004, **65**, 1121–1125.
20 P. B. Macedo, C. T. Moynihan and R. Bose, *Phys. Chem. Glasses*, 1972, **13**, 171–179.
21 C. A. Angell, *Chem. Rev.*, 1990, **90**, 523–542.
22 I. M. Hodge, M. D. Ingram and A. R. West, *J. Electroanal. Chem.*, 1976, **74**, 125–143.
23 R. Gerhardt, *J. Phys. Chem. Solids*, 1994, **55**, 1491–1506.
24 M. Ram and S. Chakrabarti, *J. Alloys Compd.*, 2008, **462**, 214–219.
25 F. Yakuphanoglu, *Physica B*, 2007, **393**, 139–142.
26 A. Dutta, T. P. Sinha, P. Jena and S. Adak, *J. Non-Cryst. Solids*, 2008, **354**, 3952–3957.
27 L. N. Patro and K. Hariharan, *Mater. Chem. Phys.*, 2009, **116**, 81–87.
28 S. B. Aziz, Z. H. Z. Abidin and A. K. Arof, *eXPRESS Polym. Lett.*, 2010, **4**, 300–310.
29 L. N. Patro and K. Hariharan, *Mater. Sci. Eng., B*, 2009, **162**, 173–178.
30 N. A. Choudhury, A. K. Shukla, S. Sampath and S. Pitchumani, *J. Electrochem. Soc.*, 2006, **153**, A614–A620.
31 V. Biju and M. A. Khadar, *J. Mater. Sci.*, 2003, **19**, 4055–4063.
32 M. Sayer, A. Mansingh, J. B. Webb and J. Noad, *J. Phys. C: Solid State Phys.*, 1978, **11**, 315–330.
33 G. J. Parravano, *J. Chem. Phys.*, 1955, **23**, 5–9.
34 A. J. Bosman and H. J. Van Daal, *Adv. Phys.*, 1970, **19**, 1–117.